Biophysical Journal
Article

Biophysical Society

Transition from Actin-Driven to Water-Driven Cell Migration Depends on External Hydraulic Resistance

Yizeng Li[1] and Sean X. Sun[1,2,3,*]
[1]Department of Mechanical Engineering, [2]Johns Hopkins Institute for NanoBioTechnology, and [3]Johns Hopkins Physical Sciences-Oncology Center, Johns Hopkins University, Baltimore, Maryland

ABSTRACT Cells in vivo can reside in diverse physical and biochemical environments. For example, epithelial cells typically live in a two-dimensional (2D) environment, whereas metastatic cancer cells can move through dense three-dimensional matrices. These distinct environments impose different kinds of mechanical forces on cells and thus potentially can influence the mechanism of cell migration. For example, cell movement on 2D flat surfaces is mostly driven by forces from focal adhesion and actin polymerization, whereas in confined geometries, it can be driven by water permeation. In this work, we utilize a two-phase model of the cellular cytoplasm in which the mechanics of the cytosol and the F-actin network are treated on an equal footing. Using conservation laws and simple force balance considerations, we are able to describe the contributions of water flux, actin polymerization and flow, and focal adhesions to cell migration both on 2D surfaces and in confined spaces. The theory shows how cell migration can seamlessly transition from a focal adhesion- and actin-based mechanism on 2D surfaces to a water-based mechanism in confined geometries.

INTRODUCTION

Animal cell migration is a complex process orchestrated by actin dynamics, focal adhesions, and also water flux (1,2). However, how these elements are added together to obtain the observed cell speed is less clear. For example, cell migration on two-dimensional (2D) surfaces is mostly driven by forces from actin polymerization and focal adhesions (3), and there has been extensive work on modeling actin-driven cell migration on 2D surfaces (4–6), whereas cells in confined geometries can be driven by water permeation (7). Moreover, cells in confined channels show a diversity of behavior: some cells such as MDA-MB-231 (human breast cancer cell line) show reduced migration speed when actin is disrupted (8,9), whereas for others such as S180 (mouse sarcoma cell line), the migration speed is unaffected (7). In addition to varying responses to actin inhibition, cell movement in confinement appears to be sensitive to hydraulic resistance (10). Even more complex are cells in three-dimensional (3D) collagen matrices, where they develop long protrusions that interact with the collagen fibers, pores, and interstitial fluid (11–15). Depending on the cell shape, the nucleus may also play a significant role in propelling the cell (16). Thus, there are diverse mechanisms driving cell migration (17). We would like to understand whether there are unified physical principles and mechanisms giving rise to the wide range of observed cell behavior. Can we explain the impact of the physical environment on the speed of cell migration? In this work, by focusing on the combined contributions from actin dynamics and water flow, we develop a general model to understand mechanisms of cell migration in 3D, 2D, and one-dimensional (1D) environments (Fig. 1, *A–C*). In all these cases, we examine an effective one-dimensional volume element of a cell and compute the leading-edge cell speed for different actin- and water-flow dynamics. We find that the hydraulic environment of the cell potentially has a counterintuitive impact on the cell speed and determines the contribution of actin and water to the observed cell movement. In particular, cells can speed up if the coefficient of external hydraulic resistance increases, even when there is no change in the molecular elements driving migration. These results explain the diversity of observed cell-migration mechanisms and suggest that cells moving in 3D matrices are not only influenced by collagen fibers but also the hydrodynamic environment.

Submitted February 1, 2018, and accepted for publication April 27, 2018.
*Correspondence: ssun@jhu.edu
Editor: Celeste Nelson.
https://doi.org/10.1016/j.bpj.2018.04.045

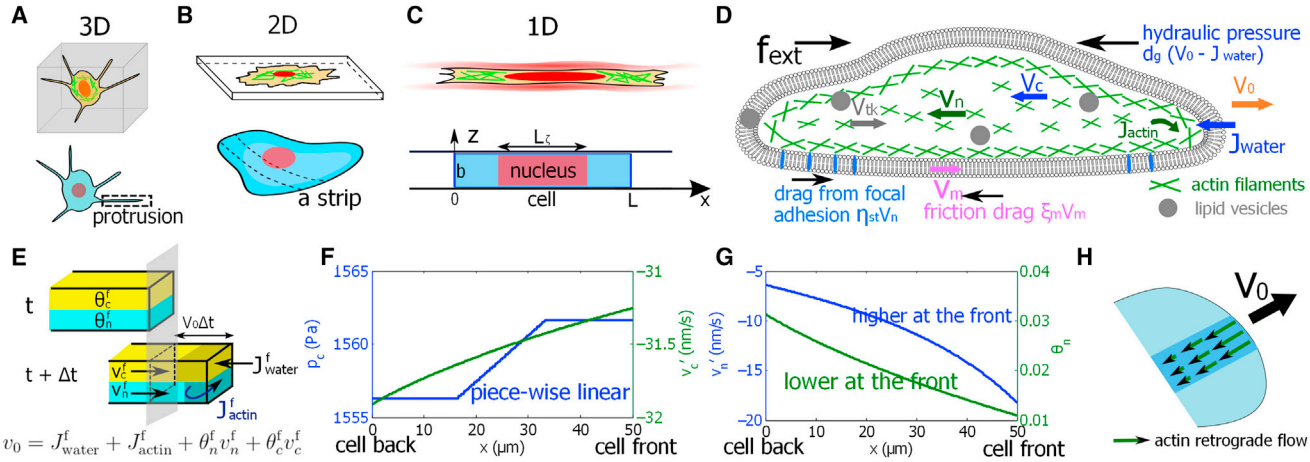

FIGURE 1 A two-fluid-phase cell-migration model. (*A*) The schematics of a cell in a 3D collagen gel are shown. The thin protrusion can be regarded as a 1D structure. (*B*) The schematics of a cell on a 2D substrate are shown. A strip of a cell on a 2D substrate can be regarded a 1D structure. (*C*) The schematics of a cell in a confined space are shown. In this case, the cell is essentially 1D. The model represents a cell (or a strip) with length L and width b. (*D*) A diagram of the relevant forces that contribute to cell migration is given. $v_{n,c}$ is the actin network and cytosol phase velocity, respectively. v_{tk} is the possible vesicle trafficking rate from the back to the front. The actin phase forms focal adhesion with the environment, resulting in a frictional drag force $\eta_{st}v_n$. Membrane movement also generates frictional force ($\xi_m v_m$). As the cell displaces external water, the hydraulic resistance can be expressed as $d_g(v_0 - J_{water})$, where v_0 is the cell boundary velocity. (*E*) A unit cross-sectional area of the cell leading edge is given. An exact kinematic relation for two-phase cell migration from time t to $t + \Delta t$ can be derived from mass balance. Each phase is attached to the cell leading edge (no void space) so that the cell velocity is related to the velocity of each phase. J^f_{actin} is the actin polymerization rate at the leading edge. J^f_{water} is the water influx rate at the leading edge. $\theta_{c,n}$ is the volume fraction of the cytosol actin network phase, respectively. v^f_c and v^f_n are the intracellular fluid velocities at the leading edge for the cytosol and actin phase, respectively. (*F*) The computed intracellular hydrostatic pressure field (*left axis*) and cytosol velocity field with respect to the cell frame (*right axis*) are shown. $v'_c = v_c - v_0$. (*G*) The computed intracellular actin velocity field with respect to the cell frame (*left axis*) and its volume fraction (*right axis*) are shown. $v'_n = v_n - v_0$. (*H*) A diagram of the actin retrograde flow predicted by the model is given. To see this figure in color, go online.

MATERIALS AND METHODS

A two-phase model of cell migration

To avoid complications associated with cell geometry, in this work, we mainly discuss a 1D-volume element of a moving cell. For example, for cells in 3D collagen matrices (Fig. 1 *A*), the thin protrusions can be regarded as 1D structures. For cells on 2D substrates (Fig. 1 *B*), we model a 1D strip of the cell. In this case, we only consider velocities and forces perpendicular to the cell leading edge. The effect of external bulk fluid flow in 2D is not considered in the model. For cells in a confined space (Fig. 1 *C*), the actin network and water flows can be directly modeled in 1D. In this case, the cell nucleus provides additional drag forces on the cytoplasm as the flows pass around or through (for the water phase) the nucleus. Within the 1D framework, the cell boundary is reduced to a front ("f") and a back ("b"). We use superscripts "f" and "b" to denote quantities associated with the cell front (leading edge) and back (trailing edge), respectively. In the following, we discuss briefly the 1D two-phase model of cell migration; more details and explanations can be found in the Supporting Materials and Methods.

In our model, we treat the cytosol (c, which is essentially water) and the actin network (n) as two fluid phases interacting with each other (18) and with the environment. The essential elements in the model are illustrated in Fig. 1 *D*. The volume fraction and velocity of the cytosol (actin network) phase are $\theta_c(\theta_n)$ and $v_c(v_n)$, respectively. In the frame of the cell body when the flow is steady, mass conservation conditions of the two phases are

$$\frac{d}{dx}\left[\theta_n v'_n\right] = 0 \tag{1}$$

and

$$\frac{d}{dx}\left[\theta_c v'_c\right] = 0, \tag{2}$$

where $v'_n = v_n - v_0$ and $v'_c = v_c - v_0$ are the velocities of the two phases in the frame of the moving cell and v_0 is the steady migration velocity of the leading edge and the cell.

For moving cells, new actin filaments are polymerized at the cell boundary with a rate $J^{f/b}_{actin}$. Similarly, water influx, $J^{f/b}_{water}$, also occurs at the cell boundary. In this model, $J^{f/b}_{actin}$ is a parameter, and $J^{f/b}_{water}$ is calculated from the chemical potential difference of water, i.e., $J^{f/b}_{water} = -\alpha^{f/b}(\Delta P^{f/b} - \Delta\Pi^{f/b})$, where $\Delta P^{f/b}$ and $\Delta\Pi^{f/b}$ are, respectively, the hydrostatic and osmotic pressure differences across the cell membrane and $\alpha^{f/b}$ is a coefficient of membrane water permeability. The cell can control $\Delta\Pi^{f/b}$ by generating ion fluxes at the cell boundary, and therefore we take it as a parameter. $\Delta P^{f/b}$ must be computed from mechanical considerations.

Because there are no void spaces, the cell boundary velocity is closely related to the boundary velocity of each phase. At the leading edge of the cell, as illustrated in Fig. 1 *E*, boundary kinematic relations read as $\theta^f_c v^f_c + J^f_{water} = v_0\theta^f_c$ and $\theta^f_n v^f_n + J^f_{actin} = v_0\theta^f_n$. Therefore, the velocity of the cell boundary is

$$v_0 = J^f_{water} + J^f_{actin} + \theta^f_n v^f_n + \theta^f_c v^f_c, \tag{3}$$

where we have used $\theta_c + \theta_n = 1$. Eq. 3 suggests that both water flux and actin polymerization can potentially contribute to cell migration (19). In a steady state with constant cell volume, $J^f_{actin} = -J^b_{actin}$ and $J^f_{water} = -J^b_{water}$; we thus use the notations $J_{actin} = J^f_{actin}$ and $J_{water} = J^f_{water}$ to represent the magnitude of these fluxes in the cell.

During cell migration, the cell membrane has a translational velocity, v_m, with respect to the surroundings. This motion leads to a frictional force between the cell and the surroundings. This force can be expressed as $f_m = -\xi_m v_m$, where ξ_m is the coefficient of frictional drag. v_m and v_0 are typically equivalent, but they can also be different if we include the velocity of membrane growth or extension from vesicle trafficking (20), v_{tk}. In this case, the apparent velocity of the cell boundary, v_0, is

formally a sum of the translational velocity of the lipid membrane and the velocity from vesicle trafficking, i.e., $v_0 = v_m + v_{tk}$. v_{tk} depends on the cell membrane tension, τ (21,22). Note that vesicle trafficking does not affect Eq. 3, which is only based on the assumption that the actin network phase is always attached to the membrane. This assumption holds during typical tissue-cell migration. One violation of such a condition is blebbing motility (23), in which the membrane extends without actin. Although blebbing motility can be analyzed within the two-phase framework, the details are more complicated. We will not discuss this case here.

If we regard the actin network as isotropic, it then also has an effective pressure that is different from the cytosol phase because of active contractions from myosin. The actin network is linked to the underlying substrate through focal adhesions and integrins (24). As the actin network flows, this linkage transmits a force from the environment to the actin network and thus onto the entire cell. For low actin-flow velocities, the force from focal adhesions is approximately proportional to the velocity of actin flow (25), i.e., $f_{st} = -\eta_{st} v_n$, where η_{st} is the coefficient of focal adhesion friction. Factors that can influence η_{st} include the substrate stiffness (26,27) and the size (28) and density (29) of adhesions. In this work, we restrict ourselves to understanding the mechanism of cell migration for a linear force-velocity relation for the focal adhesions. Experiments (25) and theory (27,30,31) have shown that the adhesion force-velocity relationship is generally complex and nonlinear. This can be incorporated into our model, but the details are not analyzed here.

To predict the cell velocity from Eq. 3, we need to know intracellular velocities v_n^f and v_c^f. These must be solved from mechanical force balance. When all of the forces are considered, the conservation of momentum for the two cytoplasmic fluid phases are

$$0 = -\theta_c \frac{d}{dx} P_c + \eta \theta_n \theta_c \left(v_n' - v_c'\right) - \zeta_c \theta_c v_c' \tag{4}$$

and

$$0 = -\theta_n \frac{d}{dx} P_c - \eta_n \theta_n \left[v_n' + (v_0 - v_m)\right] + \eta \theta_n \theta_c \left(v_c' - v_n'\right)$$

$$-\frac{d}{dx}(\theta_n \phi_n) - \eta_{st} \theta_n \left(v_n' + v_0\right) - \zeta_n \theta_n v_n', \tag{5}$$

where η is the coefficient of interphase viscous drag, η_n is the effective viscosity of the actin phase, and $\zeta_c(x)$ and $\zeta_n(x)$ are the coefficients of frictional drag from the nucleus on the cytosol and on the actin phases, respectively; these are only defined in the region where the nucleus is present. P_c and $P_n = P_c + \phi_n$ are the cytosol and network phase pressures, respectively. We write the excess pressure in the network phase as $\theta_n \phi_n$, which is also related to active contraction generated by myosin.

As the cell boundary moves at velocity v_0, the cell may experience an extracellular hydraulic resistance (in units of pressure, because this force is exerted on an area element). When $v_0 \neq J_{water}$, the cell boundary must push the external fluid at velocity $v_* = v_0 - J_{water}$. In the extreme case of a cell in a confined channel, the cell must push the complete column of water in front of the cell at the velocity v_*, and the friction between the extracellular fluid and the channel wall generates a large hydraulic resistance. This hydraulic resistance can be expressed as a linear function of v_*, i.e., $P_* = d_g(v_0 - J_{water})$, where d_g is a coefficient to be determined by the extracellular geometry and flow properties. In addition, the cell may experience external forces from extracellular objects such as mounted cantilever (32). We use f_{ext} to account for this effective force per unit area (again in units of pressure). Therefore, the force balance of the cell membrane is

$$b\left[\left(P_{in}^f - P_*^f\right) - \left(P_{in}^b - P_*^b\right)\right] + b f_{ext}^f - b f_{ext}^b = -b\eta_n \int_0^L \theta_n \left[v_n' + (v_0 - v_m)\right] dx + 2\xi_m v_m L. \tag{6}$$

The cell boundary velocity v_0 can be solved by integrating the sum of Eqs. 4 and 5 and adding that to Eq. 6. In the limit of $v_m = v_0$, v_0 can be solved analytically as follows (see Supporting Materials and Methods for more information):

$$v_0 = \frac{L\eta_{st} J_{actin} + f_{ext}^f - f_{ext}^b}{L\eta_{st}\Theta_n + 2\xi_m L/b + d_g} + \frac{L_\zeta(\zeta_c J_{water} + \zeta_n J_{actin}) + d_g J_{water}}{L\eta_{st}\Theta_n + 2\xi_m L/b + d_g}, \tag{7}$$

where L and b are the length and width of the cell (or a strip of cell), respectively, L_ζ is the length of the nucleus (Fig. 1 *C*), and Θ_n is the average volume fraction of the actin phase, satisfying $\int_0^L \theta_n(x)dx = L\Theta_n$. The approximation $v_m = v_0$ is valid when the net flux of vesicle trafficking is negligible. This can occur when the membrane-tension gradient across the cell is negligible or when the rate of vesicle formation is low. We will show that the membrane-tension gradient is indeed very small for the underlying physics included in the model. In this work, we also have not considered membrane blebbing and thus also neglect any membrane-tension changes due to blebbing (33).

The numerical values of parameters for the model are listed in Table 1. Unless otherwise specified or varied, these parameters are used throughout the work. More details on the physical interpretation of each parameter can be found in the Supporting Materials and Methods.

RESULTS AND DISCUSSION

The nucleus can increase the intracellular pressure difference

Fig. 1, *F* and *G* show a typical distribution of the intracellular hydrostatic pressure, volume fraction of the actin phase, and velocities of the two phases for a migrating cell with respect to the cell moving frame (see Supporting Materials and Methods for parameters). The velocity of the cell edge and the membrane translation are predicted to be the same, $v_0 = v_m = 12$ nm/s. Therefore, in this case, vesicle trafficking has a negligible effect. This is because the membrane tension difference between the cell front and back is negligible (see Supporting Materials and Methods and a later section). For the assumed osmotic pressure gradient, the water flux into the cell at the front is $J_{water} = 31$ nm/s, whereas the actual cell velocity is much smaller. Because $v_0 \neq J_{water}$, the cell displaces the extracellular fluid as it migrates.

The average intracellular hydrostatic pressure, P_c, is determined by the average osmolarity difference across the cell. In confined channels, the nucleus also influences P_c, giving rise to a piece-wise linear pressure profile. Larger effective drag from the nucleus on the cytosol, i.e., larger ζ_c, induces higher pressure difference between the front and back of the cell. When $\zeta_c = 0$, then P_c is a smooth function over the entire cell length, and the difference of P_c across the

TABLE 1 Parameters Used in the Models

Parameters	Description	Values	Sources
R (J/mol K)	ideal gas constant	8.31451	constant
T (K)	absolute temperature	300	room temperature
L (μm)	cell length	50	generic
L_ζ (μm)	nucleus length	$L/2$	generic
b (μm)	cell width	3	generic
h (μm)	membrane thickness	0.5	(48)
η (Pa • s/μm^2)	drag coefficient between two phases	1	(49)
η_n (Pa • s/μm^2)	effective viscosity in the actin phase	1.3	see text
ζ_c (Pa • s/μm^2)	effective drag coefficient from the nucleus to the cytosol phase	10	assumed
ζ_n (Pa • s/μm^2)	effective drag coefficient from the nucleus to the actin network phase	100	assumed
ξ_m (Pa • s/μm)	coefficient of friction of the channel wall	1	(7)
η_{st} (Pa • s/μm^2)	coefficient of drag from focal adhesion	1×10^4	(25)
d_g (Pa • s/μm)	coefficient of hydraulic pressure	1×10^3	see text
f_{ext}^f (Pa)	external force per unit area at the front	0	generic
f_{ext}^b (Pa)	external force per unit area at the back	0	generic
α^f (μm/(Pa • s))	water permeability constant at the front	1.0×10^{-4}	(7)
α^b (μm/(Pa • s))	water permeability constant at the back	1.0×10^{-4}	(7)
γ_{tk}^0 (nm/s)	maximal rate of vesicle trafficking	10	assumed
τ_{max} (Pa m)	maximal membrane tension when vesicle trafficking stops	5×10^{-2}	assumed
Θ_n	average volume fraction of the actin phase	0.02	(50)
ϕ_n (Pa)	excess pressure in the actin network	-1000 (back) to -5000 (front)	assumed
J_{actin} (nm/s)	actin flux at the two boundaries	$10\Theta_n$	assumed
P_0^f (Pa)	extracellular hydrostatic pressure at the front	0	generic
P_0^b (Pa)	extracellular hydrostatic pressure at the back	0	generic
c_0^f (mM)	extracellular ion concentration at the front	340	(7)
c_0^b (mM)	extracellular ion concentration at the back	340	(7)
c_{in}^f (mM)	intracellular ion concentration at the front	340.75	generic
c_{in}^b (mM)	intracellular ion concentration at the back	340.5	generic

These are the default parameters unless otherwise specified.

cell is reduced (see Fig. S2). This result is consistent with the "nuclear piston" mode of migration, in which the pressure gradient of the nucleus can influence cell speed (16). With the nucleus, the model predicts the same average intracellular cytosol pressure as the case without the nucleus; only $\Delta P_c = P_c^f - P_c^b$ is different. The relative velocity of the cytosol, $v_c' = v_c - v_0$ (shown in Fig. 1 *F*), is determined mostly by the boundary condition, i.e., $v_c'(L) = -J_{water}/\theta_c(L)$. Higher $|v_c'|$ at the back of the cell is consistent with the lower cytosolic volume fraction, because the product $\theta_c v_c'$ must be a constant from the mass conservation.

Retrograde flow is prominent at the cell leading edge

The relative velocity of the actin network, $v_n' = v_n - v_0$ (shown in Fig. 1 *G*), is largely determined by the rate of actin (de)polymerization at the boundaries, i.e., $v_n'(L) = -J_{actin}/\theta_n(L)$. In this example, the actin velocity at the cell front in the fixed frame is $v_n^f = v_n'^f + v_0 = -6$ nm/s. This negative velocity pointing inwards is the actin retrograde-flow motion commonly seem during cell migration (34). Our model also predicts a decrease of the retrograde velocity toward the back of the cell (Fig. 1 *G*) as seen in experiments (35). A cartoon depiction of actin retrograde flow is shown in Fig. 1 *H*. Because of the boundary condition specified in the model, we do not consider an anterograde actin flow at the back of the cell (6).

Cell migration on 2D substrates relies on actin dynamics and focal adhesion

For cells on 2D substrates, the coefficient of hydraulic resistance is negligible ($d_g^{2D} = 0$; see the Supporting Materials and Methods for more information), and the effective drag from the nucleus on the two phases can be neglected as well ($\zeta_c = \zeta_n = 0$). Hence, Eq. 7 is reduced to a simpler form in which v_0 is independent of J_{water}. The model predicts that v_0 scales with the rate of actin polymerization, J_{actin}/Θ_n, and the coefficient of focal adhesions, η_{st} (Fig. 2 *A*). In the limit of large η_{st} (for example, along the line $\eta_{st} = 10^4$ Pa • s/μm^2), the effect of ξ_m and $f_{ext}^{f/b}$ diminishes and $v_0 \simeq J_{actin}/\Theta_n$, suggesting that when the strength of focal adhesion is high (no slip), the cell velocity is determined by the rate of actin polymerization. On the other hand, when the force from focal adhesions is abolished (along the line $\eta_{st} = 1$ Pa • s/μm^2), v_0 does not increase as J_{actin} increases. This is consistent with the finding that for actin polymerization to be effective, there must be sufficient focal adhesion friction (24).

Fig. 2 *B* shows the predicted relation between v_0 and actin retrograde velocity as J_{actin} varies for different η_{st}. A higher

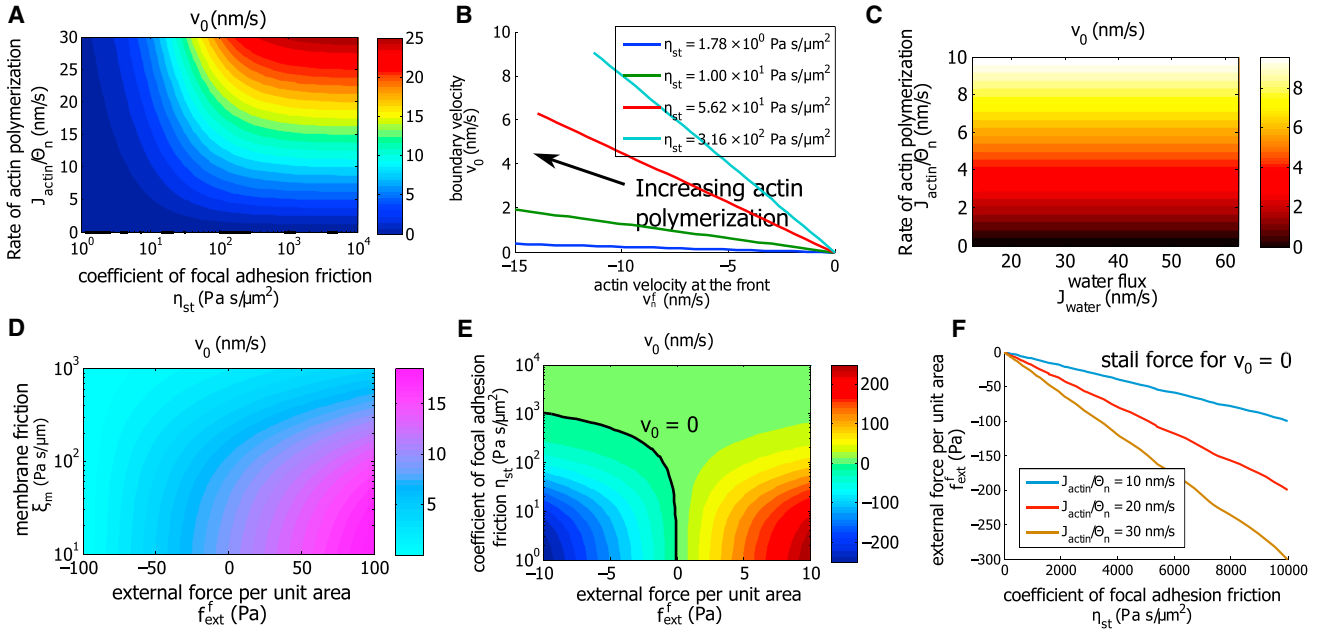

FIGURE 2 Cell migration on 2D substrates. (*A*) The contours of the cell boundary velocity, v_0, are shown as functions of actin polymerization rate J_{actin} and focal adhesion friction coefficient η_{st}. $J_{\text{actin}}/\Theta_n$ is a measure of actin velocity at the cell boundary generated by actin polymerization. In the calculation, J_{actin} varies and Θ_n remains unchanged. (*B*) The cell boundary velocity v_0 is given as a function of v_n^{f} for different coefficient of focal adhesion η_{st}. (*C*) The contours of v_0 as J_{actin} and J_{water} vary as shown. In 2D, J_{water} does not influence cell boundary velocity. (*D*) The contours of v_0 as ξ_m and $f_{\text{ext}}^{\text{f}}$ vary as shown. (*E*) The contours of v_0 as $f_{\text{ext}}^{\text{f}}$ and η_{st} vary as shown. (*F*) The stall force per unit area for different η_{st} is given. As expected, the magnitude of the stall force increases with increasing coefficients of focal adhesion friction or the rate of actin polymerization. To see this figure in color, go online.

rate of actin polymerization results in a higher cell velocity and also a higher magnitude of actin retrograde flow, because $\left|v_n^{\text{f}}\right|$ increases faster than v_0. For the same actin velocity v_n, the model predicts a higher v_0 for higher η_{st}.

Although the cell boundary velocity is in general influenced by the water flux through the membrane (Eq. 3), the model predicts that under negligible hydraulic resistance ($d_g^{\text{2D}} = 0$), the boundary velocity is independent of J_{water}. This can also be seen from Eq. 7, in which J_{water} does not contribute to v_0 when $d_g = 0$. More discussion is given in a later section.

Influence of external force on cell migration

The cell boundary moves faster if the membrane friction with the environment, $\xi_m v_m$, is low or the combination of the external forces (per unit area), $f_{\text{ext}}^{\text{f}} - f_{\text{ext}}^{\text{b}}$, points in the direction of cell migration (Fig. 2 *D*). Contour plots of v_0 as a function of η_{st} and $f_{\text{ext}}^{\text{f}}$ show a similar story (Fig. 2 *E*). We predict that when the friction force from focal adhesion is small (low η_{st}), v_0 scales linearly with $f_{\text{ext}}^{\text{f}}$; when the force from focal adhesion is large (high η_{st}), then the external forces have a negligible effect on cell velocity. Therefore, Fig. 2 *E* also implies an external force-cell velocity relation for cell migration. Similar calculations can be obtained for different rates of actin polymerization. We can extract the stall force when $v_0 = 0$ for each η_{st} and J_{actin}. As expected, the magnitude of the stall force increases as η_{st} or J_{actin} increases (Fig. 2 *F*). For a 2D cell's boundary element of 3 μm width and 200 nm height, the predicted stall force is on the order of 1 nN, which is of the same order as the stall force for cell boundary lamellipodium (32).

The spatial variation of the cell-membrane tension is set partially by the membrane friction with the environment and partially by the external force: larger ξ_m and $f_{\text{ext}}^{\text{f}} - f_{\text{ext}}^{\text{b}}$ can generate a membrane tension difference up to 10% from the back to the front of the cell (see Fig. S3). In other cases, the membrane tension is almost uniform across the cells, and thus the velocity contributed by the membrane trafficking is negligible. This result validates the assumption of $v_m = v_0$ that is used to approximate v_0 in Eq. 7. The viscosity of each phase or the friction between two phases has little contribution to v_0 (see Fig. S3), showing that for cells on 2D substrates, migration is mostly driven by actin polymerization, focal adhesion, and external forces acting on the cell.

Confined 1D cells migrate faster under higher coefficients of hydraulic resistance

For cells in confined channels (Fig. 3 *A*), the coefficient of hydraulic resistance is $d_g^{\text{1D}} = 12\mu_f \ell_0 / b^2$, where ℓ_0 is the total length of the channel and μ_f is the extracellular fluid viscosity in the channel (see the Supporting Materials and Methods for more information). A longer channel or a higher extracellular fluid viscosity leads to a higher

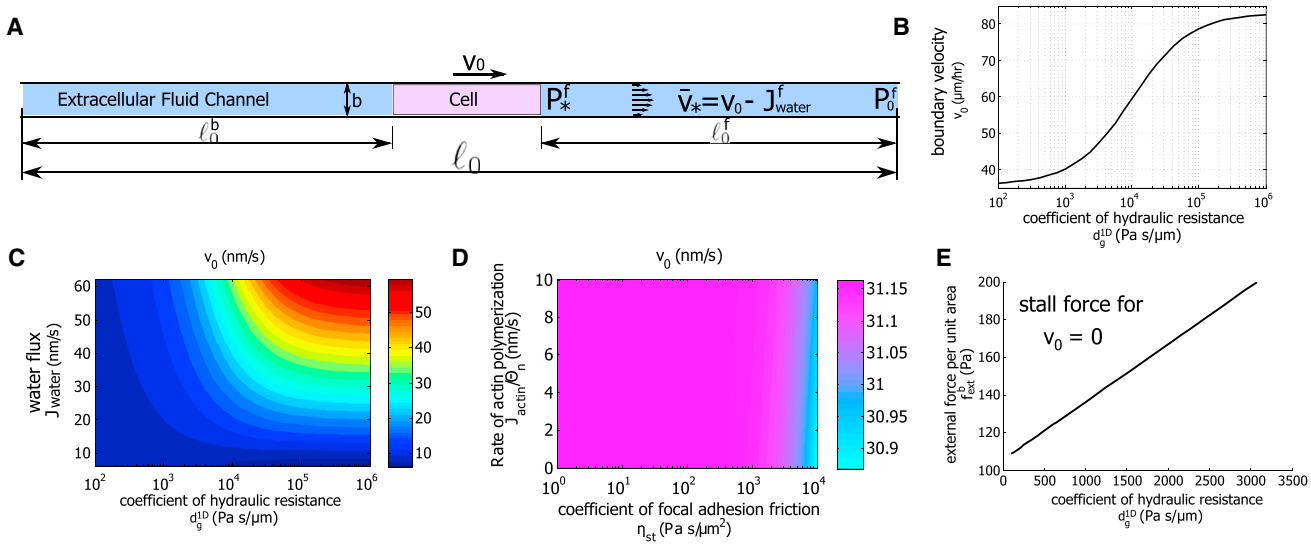

FIGURE 3 Confined 1D cells migrate faster under higher coefficients of hydraulic resistance. (*A*) A diagram of the cell and the external fluid flow in a 1D channel is shown. (*B*) A model prediction of the cell boundary velocity v_0 as d_g^{1D} varies is shown. Here, $c_{in}^f = 340.7$ mM, which corresponds to a water flux of $J_{water} = 82\ \mu$ m/h. (*C*) The velocity of the cell edge v_0 as J_{water} and d_g^{1D} vary as shown. We let c_{in}^f vary from 340.6 to 341 mM and obtain J_{water} accordingly. Cell velocity increases with increasing J_{water} and d_g^{1D}. (*D*) The contours of v_0 as J_{actin} and η_{st} vary as shown. Here, $d_g^{1D} = 10^6$ Pa•s/μm. For confined channels with high hydraulic resistance, neither actin polymerization nor focal adhesion friction influence the cell speed significantly. (*E*) Stall force per unit area increases with d_g^{1D}. To see this figure in color, go online.

coefficient of hydraulic resistance. In a typical channel in this work or in (7), for example, $b = 5\ \mu$ m, $\ell_0 = 500\ \mu$ m, and $\mu_f = 10^{-3}$ Pa • s, then d_g^{1D} is about 2.5×10^{-1} Pa • s/μm. In reality, d_g^{1D} can be much higher than this estimate because the channel walls are not smooth. Fig. 3 *B* shows the model prediction that v_0 increases with d_g^{1D} while the other parameters remain the same. The cell velocity saturates at low and high d_g^{1D}. For intermediate d_g^{1D}, one order of magnitude change of d_g^{1D}—for example, from 5×10^3 Pa • s/μm to 5×10^4 Pa • s/μm—results in an increase in cell velocity (from ~54 μm/h to ~75 μm/h) by ~40%.

This prediction, showing that cells move faster in an environment with a higher coefficient of hydraulic resistance, is rather counterintuitive. This result can be understood by considering the flow of the extracellular fluid. In Fig. 3 *B*, with constant J_{water}, v_0 increases as d_g^{1D} increases, meaning that the cell utilizes more of the water flux in v_0. This means the fluid velocity in the channel, $v_* = v_0 - J_{water}$, decreases with d_g^{1D}, which is expected under higher hydraulic resistance. In addition, the cytosol velocity v_c must be continuous with extracellular fluid velocity and decrease for larger d_g^{1D}. Therefore, the cell boundary velocity increases.

On the other hand, increased velocity of cell migration under a higher coefficient of hydraulic resistance, d_g^{1D}, helps to reduce the otherwise high hydraulic resistance, $d_g^{1D}v_*$: although the coefficient of hydraulic resistance varies from 10^2 to 10^6 Pa • s/μm, as shown in Fig. 3 *C*, the actual hydraulic resistance experienced by the cell remains in the same order of magnitude when the cell velocity v_0 increases (see Fig. S4). Note that in this work, we have assumed that the network phase is always attached to the cell boundary during continuous (de)polymerization, and the velocity of polymerization J_{actin} is constant. Experiments have shown that actin polymerization can adapt against mechanical resistance to grow at a constant velocity (36), which justifies this assumption, although, in principle, any dependence of J_{actin} on force can be incorporated in our model.

Transition between actin-driven and flow-driven cell migrations depends on the external coefficient of hydraulic resistance

Equation 3 suggests that v_0 increases with J_{water}; indeed, the model predicts that the cell migrates faster under larger water flux. Fig. 3 *C* shows the dependence of v_0 with J_{water} and d_g^{1D}. When d_g^{1D} is small ($d_g^{1D} < 10^2$ Pa • s/μm), the cell velocity is low and is almost independent of J_{water}, suggesting that water flux does not contribute to cell migration in this regime. This is the situation for cells on a 2D substrate (also see Fig. 2 *C*). When d_g^{1D} is large ($d_g^{1D} > 10^5$ Pa • s/μm), the cell velocity equals to J_{water}; this is the situation for a cell in a confined space where cell migration is mostly facilitated by water flux, i.e., an osmotic engine model (7). In this regime, the boundary velocity saturates with d_g^{1D}.

For a high coefficient of hydraulic resistance, for example, $d_g^{1D} = 10^6$ Pa • s/μm, the predicted cell velocity v_0 is independent of J_{actin} or η_{st} (Fig. 3 *D*). This result, together with Fig. 3 *C*, indicates that under a high coefficient of hydraulic resistance, v_0 is dominated by water flux, not the actin network, whereas under a low coefficient of hydraulic resistance, v_0 is dominated by the actin network, not water flux. Our model shows that the transition from

actin-driven cell migration to water-driven cell migration can result from the physical effects of fluid flow, not from a change in the mechanism of migration signaled by the cell.

Similar to the 2D case in which higher external forces are needed to stop cell migration under higher strength of focal adhesion (Fig. 2 *F*), in 1D, higher external forces are needed to stop cell migration under a higher coefficient of hydraulic resistance (Fig. 3 *E*). The magnitude of the stall force is therefore also a measure of the strength of the "driving force," which is focal adhesion and actin polymerization in 2D and water flux in 1D.

Hydraulic resistance in 3D matrices

The model can be extended to understand the influence of the hydraulic environment on cell migration in 3D matrices (hydrogels such as collagen) (Fig. 4 *A*). The front of the protrusion interacts with the matrix and the interstitial fluid. As the protrusion extends, it exerts a force on its environment and changes the hydrodynamic pressure distribution in the matrix. The extracellular matrix is a viscoelastic material with high porosity. The gel component, i.e., the collagen-fiber network, deforms as the cell protrudes and therefore exerts an external force on the migrating cell. In the case of collagen gels, the matrix is also disassembled as the cell migrates and secretes matrix metalloproteinases (37). We have seen in the previous sections that the coefficients of hydraulic resistance can vary significantly in 1D versus 2D. This difference can determine the relative contribution of different mechanisms of cell migration. In vivo, the mechanical properties of the collagen matrix are complex. Although much has been studied to understand the viscoelastic property and the porosity of the collagen matrix, it remains unclear what types of hydraulic resistance the cell experiences in 3D matrices and how this compares to the d_g in 1D and 2D. In this section, we explore how d_g in 3D depends on the mechanical properties of the collagen matrix.

Using a poroelastic theory, we estimate the effective coefficient of hydraulic resistance to be $d_g^{3D} = \mu_f b/2\kappa$ (see the Supporting Materials and Methods for more information), where μ_f is the effective viscosity of the fluid phase in the collagen matrix, κ is the permeability of the collagen matrix, and b is still the width of the cell protrusion. To differentiate the notation used in 1D, we will add "3D" or "1D" to the corresponding quantities in each geometry, i.e., $d_g^{3D} = \mu_f^{3D} b^{3D}/2\kappa$ and $d_g^{1D} = 12\mu_f^{1D}\ell_0/(b^{1D})^2$. We assume $\mu_f^{3D} = \mu_f^{1D}$. Depending on the values of $b^{3D}/2\kappa$ and $12\ell_0/(b^{1D})^2$, the coefficient of hydraulic resistance in 3D can be either larger or smaller than that in 1D. For example, when $\kappa = 10^{-16}$ m^2 (38), $b^{3D} = b^{1D} = 3$ μ m, and $\ell_0 = 10^3$ μm, then $d_g^{3D} > d_g^{1D}$. But when $\kappa = 10^{-12}$ m^2, then $d_g^{3D} < d_g^{1D}$. Fig. 4 *B* shows the phase diagram of the ratio $\ln(d_g^{1D}/d_g^{3D})$ as the 1D channel length ℓ_0 and the permeability of the collagen matrix κ vary. The line $\ln(d_g^{1D}/d_g^{3D}) = 0$ indicates $d_g^{1D} = d_g^{3D}$.

Depending on the viscosity of the interstitial fluid in the collagen matrix and the matrix hydraulic permeability, which is related to the collagen density, the coefficient of hydraulic resistance in 3D can be comparable to 1D (Fig. 4 *B*). This suggests that the hydraulic effects could play an important role in 3D cell protrusion, including morphogenesis and cancer cell metastasis. In experiments, it is found that cell velocity has a biphasic dependence on the collagen density (13), which may be attributed to collagen fiber alignment, matrix pore size (13), cell-matrix biochemical interaction, or the effect of the hydraulic resistance, which can occur when there is a large water flux through the cell surface and the hydraulic resistance starts to dominate at low matrix permeability. To fully study 3D cell migration, other matrix properties should be considered, including strain-stiffening (39), stress relaxation (40), collagen fiber alignment, matrix pore size, and production of matrix metalloproteinases (13). More extensive studies, both experimental and theoretical, are needed to address this complexity.

CONCLUSIONS

Understanding the mechanism of cell migration in different physical environments helps to uncover pathophysiological mechanisms. Using a two-phase modeling framework, we derived a general expression that is applicable to a wide range of physical conditions to compute the cell boundary velocity as a function of actin polymerization rate and water influx rate. The model incorporates

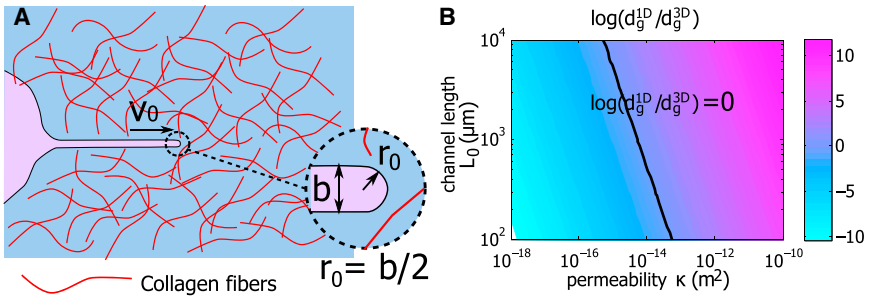

FIGURE 4 Cell movement in 3D collagen matrix. (*A*) A diagram of a cell protrusion and the surrounding collagen matrix is shown. Collagen fibers are distributed in the matrix. The tip of the protrusion has a radius $r_0 = b/2$, where b is the width of the protrusion. (*B*) The contour of $\ln(d_g^{1D}/d_g^{3D})$ as the 1D channel length ℓ_0 and the permeability of the collagen matrix κ vary is shown. The line is where $d_g^{1D} = d_g^{3D}$. To see this figure in color, go online.

known mechanics of important motility components and includes effects of focal adhesion and membrane friction force as well as hydraulic resistance from flow outside of the cell. Depending on the environmental properties, the coefficient of hydraulic resistance can be substantial, especially in 1D channels and 3D matrices. The coefficient of hydraulic resistance can influence the relative contribution of water influx to migration speed. In 2D environments, the hydraulic resistance is negligible so that even if the water influx is large, it does not contribute to cell speed as long as the cell maintains constant volume. In 1D confined channels with a high coefficient of hydraulic resistance, water influx enhances migration speed. In 3D matrices, the hydraulic resistance depends on the local environment of the cell and can be as large as the 1D case. This result suggests that in 3D, knocking out the cell components responsible for water flux would have major effects in cell motility.

In this work, we mainly focus on how cell migration may perturb the extracellular fluid environment and generate a hydraulic resistance back onto the cell; we have not considered bulk fluid flow from the environment, which can be relevant for cell migration on a 2D surface, e.g., endothelial cells in blood flow. When this bulk flow is in a confined geometry such as a blood vessel, we also expect a pressure drop in the flow and also across the cell. This hydrodynamic pressure difference across the cell can also influence cell migration. In unconfined geometries, the pressure drop across the cell is negligible during bulk flow. Instead, fluid shear stress on the cell surface is more important. This shear stress on the cell will activate membrane channels and further promote cell migration (41). A complete model incorporating effects from external bulk flow has not been developed.

Our results express the cell speed for given actin-polymerization and water-influx rates. However, exactly how these fluxes are controlled is not addressed and requires additional study and modeling. For example, the contraction of the actomyosin network is mediated by the strength of the focal adhesion. Biochemical feedback among the focal adhesion, actin flow, and actomyosin contraction can also generate traction oscillations within the adhesion (42,43). To resolve these effects, a more complicated model is needed to couple the contraction in the actomyosin network, actin flow, and the strength of adhesions. In addition, there is likely substantial cross talk between actin polymerization and water flux. Actin polymerization is linked to the polarity of the cell (44) and likely influences ion channels and pumps that set up the osmotic gradient (45). There are also direct interactions between ion channels and the cytoskeleton (46). Water and ion fluxes could also reorganize the cytoskeleton. This is especially true for calcium, which is implicated in activating myosin contraction (47). Therefore, examining the interplay between actin dynamics and water flux would yield new insights.

SUPPORTING MATERIAL

Supporting Materials and Methods and four figures are available at http://www.biophysj.org/biophysj/supplemental/S0006-3495(18)30567-8.

AUTHOR CONTRIBUTIONS

Y.L. and S.X.S. designed the theory and model, and Y.L. performed the calculations. Y.L. and S.X.S. wrote the manuscript.

ACKNOWLEDGMENTS

This work was supported by National Institutes of Health grants R01GM114675 and U54CA210172.

REFERENCES

1. Pollard, T. D., and G. G. Borisy. 2003. Cellular motility driven by assembly and disassembly of actin filaments. *Cell.* 112:453–465.
2. Tao, J., Y. Li, …, S. X. Sun. 2017. Cell mechanics: a dialogue. *Rep. Prog. Phys.* 80:036601.
3. Gardel, M. L., I. C. Schneider, …, C. M. Waterman. 2010. Mechanical integration of actin and adhesion dynamics in cell migration. *Annu. Rev. Cell Dev. Biol.* 26:315–333.
4. Barnhart, E. L., J. Allard, …, A. Mogilner. 2017. Adhesion-dependent wave generation in crawling cells. *Curr. Biol.* 27:27–38.
5. Craig, E. M., J. Stricker, …, A. Mogilner. 2015. Model for adhesion clutch explains biphasic relationship between actin flow and traction at the cell leading edge. *Phys. Biol.* 12:035002.
6. Shao, D., H. Levine, and W.-J. Rappel. 2012. Coupling actin flow, adhesion, and morphology in a computational cell motility model. *Proc. Natl. Acad. Sci. USA.* 109:6851–6856.
7. Stroka, K. M., H. Jiang, …, K. Konstantopoulos. 2014. Water permeation drives tumor cell migration in confined microenvironments. *Cell.* 157:611–623.
8. Poincloux, R., O. Collin, …, P. Chavrier. 2011. Contractility of the cell rear drives invasion of breast tumor cells in 3D Matrigel. *Proc. Natl. Acad. Sci. USA.* 108:1943–1948.
9. Carey, S. P., A. Rahman, …, C. A. Reinhart-King. 2015. Comparative mechanisms of cancer cell migration through 3D matrix and physiological microtracks. *Am. J. Physiol. Cell Physiol.* 308:C436–C447.
10. Prentice-Mott, H. V., C. H. Chang, …, J. V. Shah. 2013. Biased migration of confined neutrophil-like cells in asymmetric hydraulic environments. *Proc. Natl. Acad. Sci. USA.* 110:21006–21011.
11. Ahmadzadeh, H., M. R. Webster, …, V. B. Shenoy. 2017. Modeling the two-way feedback between contractility and matrix realignment reveals a nonlinear mode of cancer cell invasion. *Proc. Natl. Acad. Sci. USA.* 114:E1617–E1626.
12. Polacheck, W. J., A. E. German, …, R. D. Kamm. 2014. Mechanotransduction of fluid stresses governs 3D cell migration. *Proc. Natl. Acad. Sci. USA.* 111:2447–2452.
13. Fraley, S. I., P. H. Wu, …, D. Wirtz. 2015. Three-dimensional matrix fiber alignment modulates cell migration and MT1-MMP utility by spatially and temporally directing protrusions. *Sci. Rep.* 5:14580.
14. Doyle, A. D., N. Carvajal, …, K. M. Yamada. 2015. Local 3D matrix microenvironment regulates cell migration through spatiotemporal dynamics of contractility-dependent adhesions. *Nat. Commun.* 6:8720.
15. Petrie, R. J., and K. M. Yamada. 2016. Multiple mechanisms of 3D migration: the origins of plasticity. *Curr. Opin. Cell Biol.* 42:7–12.
16. Petrie, R. J., H. Koo, and K. M. Yamada. 2014. Generation of compartmentalized pressure by a nuclear piston governs cell motility in a 3D matrix. *Science.* 345:1062–1065.

17. Doyle, A. D., R. J. Petrie, …, K. M. Yamada. 2013. Dimensions in cell migration. *Curr. Opin. Cell Biol.* 25:642–649.
18. Cogan, N. G., and R. D. Guy. 2010. Multiphase flow models of biogels from crawling cells to bacterial biofilms. *HFSP J.* 4:11–25.
19. Hu, J., and A. S. Verkman. 2006. Increased migration and metastatic potential of tumor cells expressing aquaporin water channels. *FASEB J.* 20:1892–1894.
20. Fletcher, S. J., and J. Z. Rappoport. 2010. Moving forward: polarised trafficking in cell migration. *Trends Cell Biol.* 20:71–78.
21. Apodaca, G. 2002. Modulation of membrane traffic by mechanical stimuli. *Am. J. Physiol. Renal Physiol.* 282:F179–F190.
22. Diz-Muñoz, A., D. A. Fletcher, and O. D. Weiner. 2013. Use the force: membrane tension as an organizer of cell shape and motility. *Trends Cell Biol.* 23:47–53.
23. Fackler, O. T., and R. Grosse. 2008. Cell motility through plasma membrane blebbing. *J. Cell Biol.* 181:879–884.
24. Parsons, J. T., A. R. Horwitz, and M. A. Schwartz. 2010. Cell adhesion: integrating cytoskeletal dynamics and cellular tension. *Nat. Rev. Mol. Cell Biol.* 11:633–643.
25. Gardel, M. L., B. Sabass, …, C. M. Waterman. 2008. Traction stress in focal adhesions correlates biphasically with actin retrograde flow speed. *J. Cell Biol.* 183:999–1005.
26. Bangasser, B. L., G. A. Shamsan, …, D. J. Odde. 2017. Shifting the optimal stiffness for cell migration. *Nat. Commun.* 8:15313.
27. Walcott, S., and S. X. Sun. 2010. A mechanical model of actin stress fiber formation and substrate elasticity sensing in adherent cells. *Proc. Natl. Acad. Sci. USA.* 107:7757–7762.
28. Kim, D. H., and D. Wirtz. 2013. Focal adhesion size uniquely predicts cell migration. *FASEB J.* 27:1351–1361.
29. Cavalcanti-Adam, E. A., T. Volberg, …, J. P. Spatz. 2007. Cell spreading and focal adhesion dynamics are regulated by spacing of integrin ligands. *Biophys. J.* 92:2964–2974.
30. Harland, B., S. Walcott, and S. X. Sun. 2011. Adhesion dynamics and durotaxis in migrating cells. *Phys. Biol.* 8:015011.
31. Chan, C. E., and D. J. Odde. 2008. Traction dynamics of filopodia on compliant substrates. *Science.* 322:1687–1691.
32. Prass, M., K. Jacobson, …, M. Radmacher. 2006. Direct measurement of the lamellipodial protrusive force in a migrating cell. *J. Cell Biol.* 174:767–772.
33. Dai, J., and M. P. Sheetz. 1999. Membrane tether formation from blebbing cells. *Biophys. J.* 77:3363–3370.
34. Thievessen, I., P. M. Thompson, …, C. M. Waterman. 2013. Vinculin-actin interaction couples actin retrograde flow to focal adhesions, but is dispensable for focal adhesion growth. *J. Cell Biol.* 202:163–177.
35. Alexandrova, A. Y., K. Arnold, …, A. B. Verkhovsky. 2008. Comparative dynamics of retrograde actin flow and focal adhesions: formation of nascent adhesions triggers transition from fast to slow flow. *PLoS One.* 3:e3234.
36. Parekh, S. H., O. Chaudhuri, …, D. A. Fletcher. 2005. Loading history determines the velocity of actin-network growth. *Nat. Cell Biol.* 7:1219–1223.
37. Baker, B. M., and C. S. Chen. 2012. Deconstructing the third dimension: how 3D culture microenvironments alter cellular cues. *J. Cell Sci.* 125:3015–3024.
38. Vennat, E., D. Aubry, and M. Degrange. 2010. Collagen fiber network infiltration: permeability and capillary infiltration. *Transp. Porous Media.* 84:717–733.
39. Stein, A. M., D. A. Vader, …, L. M. Sander. 2011. The micromechanics of three-dimensional collagen-i gels. *Complexity.* 16:22–28.
40. Nam, S., K. H. Hu, …, O. Chaudhuri. 2016. Strain-enhanced stress relaxation impacts nonlinear elasticity in collagen gels. *Proc. Natl. Acad. Sci. USA.* 113:5492–5497.
41. Shiu, Y. T., S. Li, …, S. Chien. 2004. Rho mediates the shear-enhancement of endothelial cell migration and traction force generation. *Biophys. J.* 86:2558–2565.
42. Plotnikov, S. V., A. M. Pasapera, …, C. M. Waterman. 2012. Force fluctuations within focal adhesions mediate ECM-rigidity sensing to guide directed cell migration. *Cell.* 151:1513–1527.
43. Wu, Z., S. V. Plotnikov, …, J. Liu. 2017. Two distinct actin networks mediate traction oscillations to confer focal adhesion mechanosensing. *Biophys. J.* 112:780–794.
44. Lomakin, A. J., K. C. Lee, …, G. Danuser. 2015. Competition for actin between two distinct F-actin networks defines a bistable switch for cell polarization. *Nat. Cell Biol.* 17:1435–1445.
45. Rosado, J. A., S. Jenner, and S. O. Sage. 2000. A role for the actin cytoskeleton in the initiation and maintenance of store-mediated calcium entry in human platelets. Evidence for conformational coupling. *J. Biol. Chem.* 275:7527–7533.
46. Schwab, A., A. Fabian, …, C. Stock. 2012. Role of ion channels and transporters in cell migration. *Physiol. Rev.* 92:1865–1913.
47. Veksler, A., and N. S. Gov. 2009. Calcium-actin waves and oscillations of cellular membranes. *Biophys. J.* 97:1558–1568.
48. Jiang, H., and S. X. Sun. 2013. Cellular pressure and volume regulation and implications for cell mechanics. *Biophys. J.* 105:609–619.
49. Dembo, M., and F. Harlow. 1986. Cell motion, contractile networks, and the physics of interpenetrating reactive flow. *Biophys. J.* 50:109–121.
50. Satcher, R. L., Jr., and C. F. Dewey, Jr. 1996. Theoretical estimates of mechanical properties of the endothelial cell cytoskeleton. *Biophys. J.* 71:109–118.